Title

SP3-Enabled Rapid and High Coverage Chemoproteomic Identification of Cell-State–Dependent Redox-Sensitive Cysteines

Journal

Molecular & Cellular Proteomics, 21(4)

ISSN

1535-9476

Authors

Desai, Heta S
Yan, Tianyang
Yu, Fengchao
et al.

Publication Date

2022-04-01

DOI

10.1016/j.mcpro.2022.100218

Peer reviewed

SP3-Enabled Rapid and High Coverage Chemoproteomic Identification of Cell-State–Dependent Redox-Sensitive Cysteines

Authors

Heta S. Desai, Tianyang Yan, Fengchao Yu, Alexander W. Sun, Miranda Villanueva, Alexey I. Nesvizhskii, and Keriann M. Backus

Correspondence

kbackus@mednet.ucla.edu

Graphical Abstract

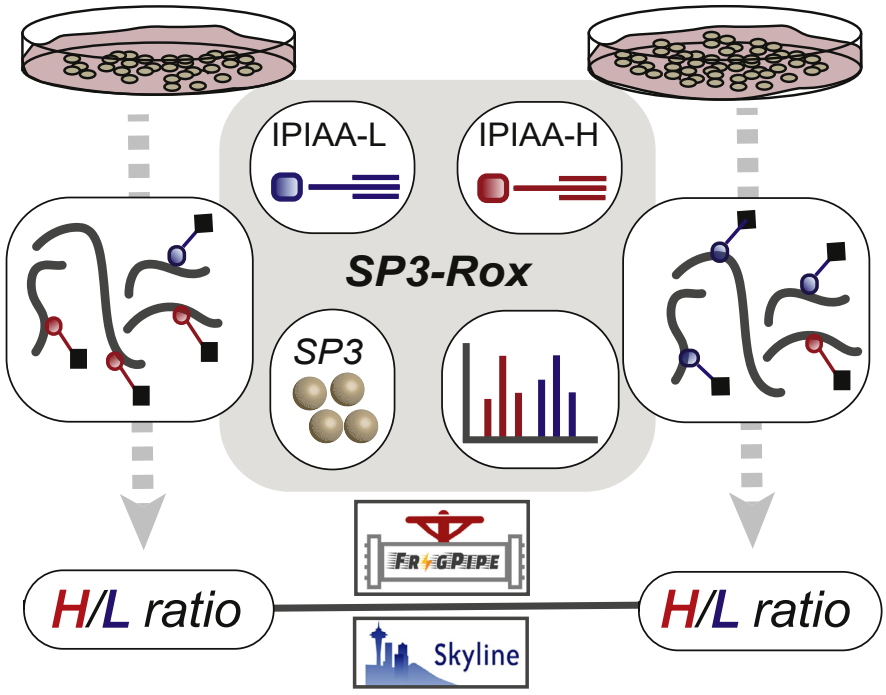

In brief

Oxidative stress has been implicated in most biological processes. To improve our understanding of how cells are impacted by and respond to oxidative stressors, we developed a new proteomics method, SP3-Rox that can accurately quantify the oxidation state of thousands of cysteines proteome-wide. We establish the MSFragger algorithm as a computational platform capable of quantifying changes to thiol oxidation, including for peptides containing multiple cysteines. Application of SP3-Rox uncovered cell-state–dependent redox-sensitive residues in primary human T cells.

Highlights

- High-coverage Cys oxidation state quantification using custom isotopic probes.
- FragPipe-IonQuant accurately quantifies Cys labeling comparably to Skyline.
- PTMProphet enables site-of-labeling localization for multi-Cys–containing peptides.
- SP3-Rox identifies changes in Cys oxidation during T cell activation.

2022, Mol Cell Proteomics *21*(*4*), 100218

https://doi.org/10.1016/j.mcpro.2022.100218

SP3-Enabled Rapid and High Coverage Chemoproteomic Identification of Cell-State–Dependent Redox-Sensitive Cysteines

Heta S. Desai[1,2], Tianyang Yan[1,3], Fengchao Yu[4], Alexander W. Sun[1], Miranda Villanueva[1,2], Alexey I. Nesvizhskii[5,4], and Keriann M. Backus[1,3,2,6,7,8,*]

Proteinaceous cysteine residues act as privileged sensors of oxidative stress. As reactive oxygen and nitrogen species have been implicated in numerous pathophysiological processes, deciphering which cysteines are sensitive to oxidative modification and the specific nature of these modifications is essential to understanding protein and cellular function in health and disease. While established mass spectrometry-based proteomic platforms have improved our understanding of the redox proteome, the widespread adoption of these methods is often hindered by complex sample preparation workflows, prohibitive cost of isotopic labeling reagents, and requirements for custom data analysis workflows. Here, we present the SP3-Rox redox proteomics method that combines tailored low cost isotopically labeled capture reagents with SP3 sample cleanup to achieve high throughput and high coverage proteome-wide identification of redox-sensitive cysteines. By implementing a customized workflow in the free FragPipe computational pipeline, we achieve accurate MS1-based quantitation, including for peptides containing multiple cysteine residues. Application of the SP3-Rox method to cellular proteomes identified cysteines sensitive to the oxidative stressor GSNO and cysteine oxidation state changes that occur during T cell activation.

Oxidative stress plays an essential role in human health and disease. Both reactive oxygen species (ROS) and reactive nitrogen species (RNS) have been implicated in many pathophysiological processes, including cancers, neurodegenerative disorders, and atherosclerosis (1–3). Oxidative stress also plays an essential role in the modulation of innate and adaptive immune responses, with abnormal cellular activation occurring at both hypo- and hyper-levels of ROS and RNS (4–6). Consequently, the identification of mechanisms by which cells respond to oxidative stressors is an essential step to improving the treatment and prevention of a wide range of human disorders.

Inherently nucleophilic and sensitive to oxidative stress, proteinaceous cysteine residues function as key sensors of ROS and RNS through oxidative modifications, including disulfide formation, S-nitrosation, and sulfenylation (3, 7). Therefore, the proteome-wide identification of redox-sensitive cysteine residues has emerged as a useful strategy to gain insight into cellular response to oxidative stress (8). Numerous proteomic methods, including OxiCat, Biotin Switch, and modifications to these methodologies (8–14) have enabled the high throughput identification of cysteines sensitive to oxidative modifications. Exemplifying these technical innovations, recent application of isobaric mass tagging coupled with immobilized metal affinity chromatography to the organism-wide identification of redox-sensitive cysteines identified ~34,000 unique cysteines across 10 murine tissues (15).

Most of these platforms rely upon the same general workflow: first, all reduced cysteines are capped using a cysteine reactive probe such as iodoacetamide (IA). After removal of all excess IA, oxidized cysteines are then reduced by the application of reducing agents tailored to the oxidized species of interest (*e.g.*, gentler reductant such as sodium ascorbate for selective identification of nitrosylated cysteines or stronger reducing agents such as tris(2-carboxyethyl)phosphine (TCEP) or DTT for identification of all oxidized cysteines, including disulfides and sulfenylated cysteines) (11, 16–18). Newly liberated thiol side chains are then capped using a second cysteine-reactive electrophile, typically one that features an enrichment handle (*e.g.*, iodoacetamide alkyne (IAA) or iodoacetamide-desthiobiotin). After enrichment and proteolytic digestion, oxidized cysteines are then identified using standard LC-MS/MS analysis workflows. Incorporation of isotopic labeling strategies, including stable isotope labeling

From the [1]Biological Chemistry Department, David Geffen School of Medicine, [2]Molecular Biology Institute, and [3]Department of Chemistry and Biochemistry, UCLA, Los Angeles, California, USA; [4]Department of Pathology, and [5]Department of Computational Medicine and Bioinformatics, University of Michigan, Ann Arbor, Michigan, USA; [6]DOE Institute for Genomics and Proteomics, [7]Jonsson Comprehensive Cancer Center, and [8]Eli and Edythe Broad Center of Regenerative Medicine and Stem Cell Research, UCLA, Los Angeles, California, USA
*For correspondence: Keriann M. Backus, kbackus@mednet.ucla.edu.

https://doi.org/10.1016/j.mcpro.2022.100218

by amino acids in cell culture and other isotopic labeling reagents, such as isotope-coded affinity tag reagents, tandem mass tag labeling reagents, isobaric tags for relative and absolute quantification, and heavy- and light-IAA, enables inter- and intra-sample quantitation of relative and absolute cysteine oxidation (9, 15, 19–23).

While already widely adopted, redox proteomic methods suffer from several shared limitations. Reliance on costly isotopically labeled reagents has made large scale redox studies cost-prohibitive for many groups. Efficient removal of excess cysteine-labeling reagent, which is essential to achieving high fidelity identification of redox-sensitive cysteines, requires laborious sample decontamination steps, such as protein precipitation or buffer exchange. Such sample manipulation can easily result in material loss or spurious results due to inefficient decontamination. The large amount of sample input required for most redox proteomic methods has hindered application to samples with limited available material, such as primary cells and biopsy samples.

Several hurdles also exist for quantitative analysis of redox proteomics datasets. Accurate quantitation (frequently at the MS1 level) is an essential component of most chemoproteomic data analysis workflows, including methods aimed at measuring thiol oxidation state. Prior studies, including our own, have relied upon custom software to report accurate measures of relative MS1 chromatographic peak areas for the extracted ion chromatograms of heavy- and light-reagent–labeled peptides. While some commercial software packages, such as ProLuCID/Census and Byonic have been successfully employed for residue-level quantification of chemoproteomics experiments, the cost of these tools has precluded widespread adoption (24). Powerful free software packages for both data search and quantitation, including Skyline and FragPipe, have been widely employed by the mass spectrometry community (25–34). However, the adoption of these tools for chemoproteomics remains limited to a handful of studies, due in part to incompatibility with several specific applications, including the quantification of peptides containing multiple modifications (*e.g.*, peptides with two or more cysteine residues). As multi-cysteine-containing peptides are ubiquitous in redox motifs (*e.g.*, CXXC), this limitation is particularly problematic for measures of thiol-oxidation state (35–37). Furthermore, the relative performance of these tools for chemoproteomic applications remains unexplored.

An optimal redox proteomic method would achieve near complete removal of excess reagents with minimal sample loss, be compatible with all cell and tissue types, use a minimal amount of input material, report oxidative modifications with high sensitivity and specificity, and be cost-effective. The single-pot, solid-phase-enhanced sample-preparation (SP3) method is poised to enable such a method. The single-pot, solid-phase-enhanced sample-preparation method employs carboxyl-coated magnetic beads to achieve efficient sample decontamination, even for small sample sizes (38, 39). Our recent findings revealed that not only is SP3 compatible with cysteine chemoproteomics, it even affords improved coverage of labeled peptides when benchmarked against protein-precipitation-based cleanup methods (40). SP3 also facilitates multiple rounds of sample cleanup, using a simple magnetic capture and elution system. Whether SP3 can enable identification of redox sensitive cysteines remains unexplored.

To enable rapid, cost-effective, and high throughput redox proteomics, we first synthesized novel and low-cost isotopically labeled IAA probes. We then combined these reagents with a new multi-step SP3 redox sample preparation workflow (SP3-Rox) compatible with FragPipe-IonQuant based quantification to achieve rapid and high coverage identification of redox-sensitive cysteines. We validate the accuracy of IonQuant quantification by comparison to widely adopted Skyline-based MS1 level quantification. Application of the SP3-Rox method identified redox sensitive cysteines sensitive to S-nitrosoglutathione (GSNO) in proteomes derived from an immortalized T lymphocyte cell line and cysteines in primary human T cells that showed cell-state dependent oxidation states. The technical innovations and expanded portrait of the redox proteome enabled by SP3-Rox provides a roadmap for a proteome-wide understanding of the cellular mechanisms underlying response to oxidative stress.

EXPERIMENTAL PROCEDURES

Experimental Design and Statistical Rationale

We used a total of 58 datasets in this work. In all datasets, we estimated the identification false-discovery rate using the target-decoy approach (41). For MSFragger, peptide-spectrum matches (PSMs), peptides, and proteins were filtered at 1% PSM and 1% protein identification FDR. For Skyline analyses, default settings were used unless otherwise noted. All experiments were performed in duplicate or triplicate for quantification accuracy assessment and method validation. S-nitrosoglutathione and T cell experiments utilized experimental duplicates with two additional technical replicates per condition (n = 4 for ± GSNO and resting/activated T cells). Aggregated mean $\log_2$(heavy:light ratios) were used to assess peptide quantification accuracy in comparison to ground-truth ratios. Comparison of the number of unique quantified cysteine-containing peptides was used to evaluate the performance of quantitation pipelines. Means of reported $\log_2$ ratio values for each condition (± GSNO or unstimulated/stimulated T cells) were calculated for all replicates per condition, and the difference of the $\log_2$ mean values were reported. Variances were calculated for each sample-condition pairing and a corresponding two-sample *t* test was performed on the raw $\log_2$ ratios to generate *p*-values (n = 4 for ± GSNO and unstimulated/stimulated T cells); *p*-values were adjusted for multiple comparisons using Benjamini–Hochberg procedure. Quantified peptides identified in all replicate samples per condition for ± GSNO and unstimulated/stimulated T cell experiments were used for statistical analyses. Difference values above 2 and 1.5 were used in subsequent gene ontology and expression analyses for GSNO and T cell experiments respectively.

Cell Culture and Preparation of Cell Lysates

All cell lines were obtained from ATCC and maintained at a low passage number (<20 passages) and tested regularly for *mycoplasma*. The cells were cultured in DMEM/RPMI-1640 supplemented with 10 % fetal bovine serum and penicillin-streptomycin. Media was filtered (0.22 μm) prior to use. Cells were maintained in a humidified incubator at 37 °C with 5 % CO2. Cells were harvested by centrifugation, washed twice with cold DPBS, resuspended in DPBS, and sonicated. Blood from deidentified healthy donor was obtained from UCLA/CFAR Virology Core (5P30 AI028697) after informed consent. After Trima filter isolation, peripheral blood mononuclear cells were purified over Ficoll–Hypaque gradient (Sigma-Aldrich), and T cells were isolated *via* negative selection with magnetic beads (EasySep Human T Cell Iso Kit, 17951, STEMCELL). The isolated T cells were washed with sterile PBS. Unstimulated cells were harvested by centrifugation. The remaining cells were then resuspended in RPMI-1640 supplemented with FBS, penicillin, streptomycin, and glutamine (2 million cells per ml), and 200,000 cells per well were seeded on nontreated tissue culture, 96-well transparent plates that had been coated with anti-CD3 (1:200, BioXcell) and anti-CD28 (1:500, Biolegend) in PBS (100 μl per well). After 72 h, the cells were then harvested, washed with PBS, and the cell pellets lysed by sonication in PBS. Protein concentrations were determined using a Bio-Rad DC protein assay kit from Bio-Rad Life Science, and the lysate diluted to the working concentrations as indicated.

Gel-Based Proteome Labeling

HEK293T proteome (25 μl of 2 mg/ml) was labeled with 30 μM isopropyl iodoacetamide alkyne (IPIAA)-H (5), IPIAA-L (4), or IAA (6) (0.75 μl of 1 mM stocks) for 1 h. Copper-catalyzed azide–alkyne cycloaddition (CuAAC) was performed with rho-azide (#) (1 μl of 1.25 mM stock in DMSO, final concentration = 50 μM), TCEP (0.5 μl of fresh 50 mM stock in water, final concentration = 1 mM), tris((1-benzyl-4-triazolyl)methyl)amine (1.5 μl of 1.7 mM stock in DMSO/*t*-butanol 1:4, final concentration = 100 μM), and $CuSO_4$ (0.5 μl of 50 mM stock in water, final concentration = 1 mM). Samples were allowed to react for 1 h at ambient temperature. All samples were denatured (5 min, 95 °C) and analyzed by SDS-PAGE using Criterion TGX Stain-free gels obtained from Bio-Rad. Loading control images were obtained after Coomassie staining.

SP3-Rox Proteomic Sample Preparation

Details for each experiment are provided in Supporting Information. Lysate samples (200 μl of 2 mg/ml) were incubated with vehicle or 1 mM GSNO for 30 min at room temperature (RT) followed by labeling with 2 mM IPIAA-L (4; 2 μl of 200 mM stock solution in DMSO, final concentration = 2 mM) for 1 h at 37 °C. The samples were incubated with 0.5 μl benzonase (Fisher Scientific, 70–664–3) for 30 min at 37 °C. SP3 bead slurries were then transferred to the proteome samples, incubated for 10 min at RT with shaking (1000 rpm). Absolute ethanol (400 μl) was added to each sample, and the samples were incubated for 5 min at RT with shaking (1000 rpm). Using the magnetic rack as described above, supernatants were then removed and discarded and the beads were further washed two times with 80% ethanol in water (400 μl). Beads were then resuspended in 200 μl PBS containing 2 M urea. TCEP (10 μl of 100 mM stock in water, final concentration = 5 mM) was added into each sample, and the sample was incubated at 56 °C for 30 min, shaking (500 rpm). Beads were washed with absolute ethanol for 5 min followed by 80% ethanol twice as described and resuspended in 200 μl PBS containing 2 M urea. The samples were then labeled with IPIAA-H (5; 2 μl of 200 mM stock solution in DMSO, final concentration = 2 mM) for 1 h at 37 °C with shaking (500 rpm). Absolute ethanol (400 μl) was added to each sample, and the samples were incubated for 5 min at RT with shaking (1000 rpm). Samples were then placed on a magnetic rack, and the beads are allowed to settle. Supernatants were then removed and discarded. Beads were then resuspended in 200 μl 0.5% SDS in PBS. Copper-catalyzed azide–alkyne cycloaddition was performed with biotin-azide 7 (4 μl of 200 mM stock in DMSO, final concentration = 4 mM), TCEP (4 μl of fresh 50 mM stock in water, final concentration = 1 mM), tris((1-benzyl-4-triazolyl)methyl)amine (12 μl of 1.7 mM stock in DMSO/*t*-butanol 1:4, final concentration = 100 μM), and $CuSO_4$ (4 μl of 50 mM stock in water, final concentration = 1 mM). Samples were allowed to react for 1 h at ambient temperature with shaking (500 rpm). Samples were washed and subjected to trypsin digestion as described below.

SP3 Digest and Elution

Absolute ethanol (400 μl) was added to each sample, and the samples were incubated for 5 min at RT with shaking (1000 rpm). Beads were washed with 80% ethanol as described above. The beads were then resuspended in 200 μl 0.5% SDS in PBS containing 2 M urea. Dithiothreitol (DTT; 10 μl of 200 mM stock in water, final concentration = 10 mM) was added into each sample, and the sample was incubated at 65 °C for 15 min. To this, iodoacetamide (10 μl of 400 mM stock in water, final concentration = 20 mM) was added and the solution was incubated for 30 min at 37 °C with shaking. After that, beads were washed with ethanol as described. Next, the beads were resuspended in 150 μl PBS containing 2 M urea followed by an addition of 3 μl trypsin 1 mg/ml solution. Digest was allowed to proceed overnight at 37 °C with shaking. After digestion, ~4 ml acetonitrile was added to each sample and the mixtures were incubated for 10 min at RT with shaking (1000 rpm). Supernatants were then removed and discarded using the magnetic rack, and the beads were washed (3 × 1 ml acetonitrile). Peptides were then eluted from SP3 beads with 100 μl of 2% DMSO in molecular biology (MB) grade water for 30 min at 37 °C with shaking two times for a total of 200 μl eluent.

NeutrAvidin Enrichment of Labeled Peptides

For each sample, 50 μl of NeutrAvidin Agarose resin slurry (Pierce) was washed three times in 10 ml immunoaffinity purification buffer (50 mM MOPS–NaOH (pH 7.2), 10 mM Na_2HPO_4, 50 mM NaCl) and then resuspended in 500 μl immunoaffinity purification buffer. Peptide solutions eluted from SP3 beads were then transferred, and the samples were then rotated for 2 h at RT. After incubation, the beads were pelleted by centrifugation and washed. Bound peptides were eluted with 60 μl of 80 % acetonitrile in MB water containing 0.1% formic acid (10 min at RT & 10 min at 72 °C). The eluants were dried (SpeedVac). The samples were then reconstituted with 5% acetonitrile and 1% formic acid in MB grade water and analyzed by LC-MS/MS.

LC-MS/MS Analysis

Details are provided in Supporting Information document. The samples were analyzed by liquid chromatography tandem mass spectrometry using Orbitrap Eclipse Tribrid Mass Spectrometer (Thermo Scientific) coupled to an Easy-nLC 1200 system.

FragPipe Peptide Identification and Quantitation

Details are provided in Supporting Information document and workflow file in PRIDE (PXD029500). Raw data collected by LC–MS/MS were converted to mzML format (for PTMProphet datasets) or left as raw files and searched using FragPipe GUI v16.0 with MSFragger (version 3.3) (28, 32), Philosopher (version 4.0.0) (34) and IonQuant (version 1.7.5) (29, 30) were enabled. Precursor and fragment mass tolerance was set as 20 ppm. Missed cleavages were allowed up to 2. Peptide length was set 7 to 50, and peptide mass range was set 500 to 5000. Cysteine residues were searched with variable

modifications at cysteine residues for carboxyamidomethylation (+57.02146), IPIAA-L (+463.2366), and IPIAA-H (+467.2529) labeling allowing for 3 max occurrences and all mods used in first search checked. Peptide and protein level FDR were set to 1%. Permissive IonQuant parameters allowed minimum scan/isotope numbers set to 1. PTMProphet information was obtained from psm.tsv using 'heavy' and 'light' localizations scores. A FASTA database from UniProtKB *homo sapien* FASTA file containing canonical, nonredundant sequences (08/2018) used for all searches and is provided in the PRIDE (PXD029500 and PXD031647) repository. Proteomic workflow of FragPipe and its collection of tools are outlined in Supporting Information.

Skyline Quantitation

Details are provided in Supporting Information document. Interact.pep.xml files from FragPipe searches were imported into Skyline v21.1.0.146 (42) with a probability threshold corresponding to the 1% peptide-ion level FDR in the dataset. Following the standard DDA analysis workflow for isotopically labeled dataset using the following modifications: carboxyamidomethylation (+57.02146) as a variable modification, light structural modification (+463.2366), and heavy isotope modification (+4.01634). As Skyline automatically places a heavy isotopic label on all modified cysteines, including carbamidomethylated residues and those modified by the IPIAA-H regent, quantification fails for peptides containing two or more modified cysteines (*e.g.*, one carbamidomethyl residue and one IPIAA-residue). A custom plugin was generated to remove the heavy mass from all carbamidomethylated residues.

Data Analysis and Processing

Custom R scripts were implemented to compile labeled peptide datasets from peptide_label_quant.tsv FragPipe outputs. Unique cysteines were quantified for each dataset using unique identifiers consisting of UniprotID_Cysteine Number. Details of data processing are in Supplemental Information.

Synthesis of Reagents

Compound 6 and 7 were prepared as has been reported (43). Detailed syntheses of compounds 4 and 5 are provided in the electronic Supplementary Information.

RESULTS

Synthesis and Benchmarking of Low-Cost Isotopically Labeled IAA Probes

Relatively cost-effective isotopically labeled IAA probes have been achieved, using ^{13}C-benzaldehyde ($115/mmol) as a low-cost isotope source (9). Here, we envisioned the synthesis of even lower cost second generation IAA probes, by employing isotopically labeled ^{13}C-acetone ($60/mmol) for isotopic barcoding. The desired light and heavy isopropyl iodoacetamide probes (IPIAA-L and IPIAA-H) were obtained in three steps, and the key isotopic labels were incorporated by reductive alkylation with propargyl amine and acetone, using either ^{12}C- or ^{13}C-acetone and $NaBH_3CN$ or $NaBD_3CN$ for the light and heavy probes, respectively, as shown in Figure 1*A*. Analysis of the reagents by LC-MS confirmed that the desired isotopologues had been obtained at equal concentrations (Fig. 1*B*).

With probes validated, we next established labeling conditions to achieve high occupancy cysteine capping required for redox proteomics. Benchmarking of the IPIAA probes against a standard unsubstituted IAA probe using a gel-based assay revealed comparable labeling and banding pattern for all three probes (Fig. 1*C*). Using a competitive gel-based assay under denaturing conditions (2M Urea), we found that at 2 mM concentration, all three probes efficiently blocked lysate labeling by IA-rhodamine. This finding concurs with our prior study (40), which indicated that low mM concentrations of iodoacetamide reagents are sufficient to cap most cysteines with near completion (supplemental Fig. S1). Somewhat unexpectedly, a comparison of cysteine labeling at pH 7 and pH 8.4 revealed near complete competition of IA-rhodamine labeling at both neutral and more basic pH (supplemental Fig. S2). Next, we carried out a mass spectrometry-based competitive assay by subjecting Jurkat lysates to labeling with 2 mM IPIAA-H and IPIAA-L probes followed by 20 mM IA to completely cap all unlabeled cysteines. After tryptic digest and LC-MS/MS analysis, search using MSFragger revealed that for both the light and heavy probes, >80% of all cysteines were labeled with the IPIAA (supplemental Fig. S3). The observed slight decrease in labeling efficiency compared to our prior study using unsubstituted IAA (40) can likely be ascribed to the increased steric bulk afforded by the isopropyl modification.

FragPipe-IonQuant and Skyline-Based Quantitation for Chemoproteomic Analysis

With probes in hand, we sought to establish a robust platform for chemoproteomic dataset quantitation. We subjected HEK293T cell lysates to labeling with different ratios of the IPIAA-H and IPIAA-L probes (1:1 and 4:1) (Fig. 2*A*). The heavy- and light-labeled samples were then subjected to CuAAC to biotin-azide, SP3 sample cleanup, on-resin digest, enrichment on Neutravidin, and LC-MS/MS analysis. Guided by the precedent of recent reports, including our prior study (40) that showcased the compatibility of MSFragger - ultrafast, easy-to-use search algorithm - with chemoproteomics, we opted to use FragPipe - the MSFragger-powered computational pipeline for proteomics data analysis. In a conventional 'closed' MSFragger search with FragPipe v16.0, we identified 8,350 cysteine-containing peptides, 7,126 light-labeled, and 4,017 heavy-labeled peptides in one 1:1 (H:L) replicate.

Next, we sought to identify a quantitation algorithm compatible with our SP3-Rox method, including for multi-cysteine containing peptides. While there are many available quantitation algorithms, we opted to compare FragPipe's built-in IonQuant tool (29, 30) to the quantitation achieved by Skyline v21.1.0.146 (42). These packages were selected based on widespread adoption by the proteomics community and availability of options for compatibility with multi-cys containing peptides and with Field Asymmetric Ion Mobility Spectrometry (FAIMS) data (44). To quantify data in FragPipe,

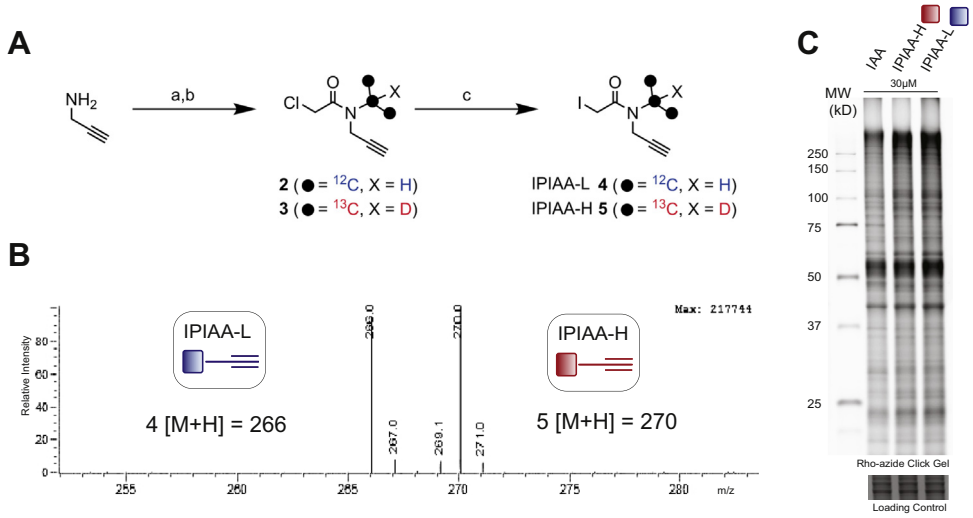

FIG. 1. **Synthesis and evaluation of isotopic isopropyl iodoacetamide alkyne probes.** *A*, synthesis of heavy and light iodoacetamide alkyne probes. a, acetone (^{13}C or light), $NaBH_3CN$ or $NaBD_3CN$, CH_2Cl_2/MeOH (2:1); rt b, chloroacetyl chloride, NEt_3; c, NaI, acetone, CH_2Cl_2, 6.2% yield for 4 over 3 steps, 11% yield for 5 over 3 steps, and 11% yield for 5 over 3 steps. *B*, LC-MS of IPIAA probes in equimolar mixture. *C*, gel-based visualization of 30uM IPIAA labeling followed by CuAAC to rhodamine-azide in HEK293T lysates. Loading control was generated using InstantBlue Coomassie protein stain. CuAAC, copper-catalyzed azide–alkyne cycloaddition; IAA, iodoacetamide alkyne; IPIAA, isopropyl iodoacetamide alkyne.

we customized a workflow (see Supplemental Information) that substantially increased the fraction of peptides quantified when compared to the default settings (supplemental Fig. S5). One key modification that was implemented was selection of the "use all mods in first search" that retains all modifications from the user's setting in the initial search, which enables improved mass calibration for peptides. Without this option, MSFragger only keeps common modifications in the first search; for samples with rare modifications, the number of high quality PSMs would be insufficient for mass calibration.

We quantified 5748, 5736, and 8269 cysteines in the 1:1, 4:1, and 1:10 (H:L) datasets respectively with IonQuant (Figs. 2 and S4), where at least 93% of all peptides identified fall within ratio windows [$1 > \log_2(H/L) > -1$, $4 > \log_2(H/L) > 1$, and $1 > \log_2(H/L) > -4$], supporting accurate quantification of labeled cysteines. More variability in ratios was observed for the 1:10 datasets consistent with decreased accuracy for larger fold change MS1 chromatographic peak area ratios. We also observed a marked increase in the fraction of peptides detected with only one isotopic label (*e.g.*, only heavy-label identified) for higher reagent ratio combinations (Fig. 2*C*). We found for 1:10 samples, ~1,200 unique cysteines and for 4:1 samples ~100 unique cysteines with single labels (Figs. 2*C* and S4). For these peptides, we set the ratio value to a

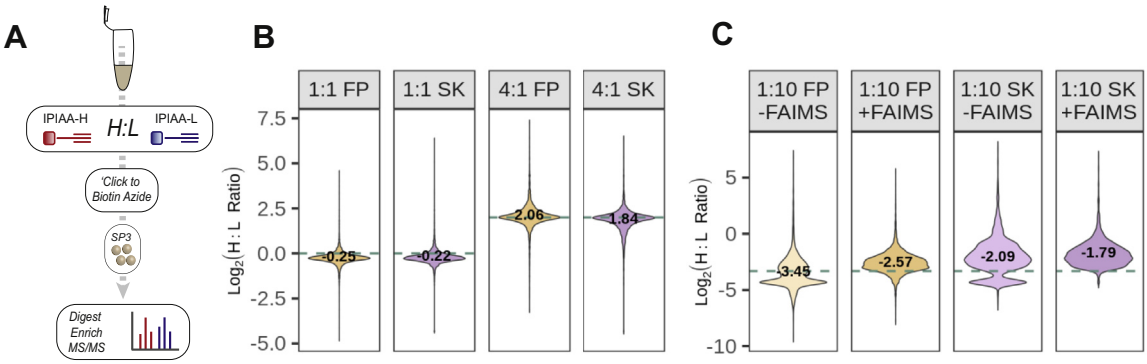

FIG. 2. **Quantification of IPIAA probes in various heavy to light ratios using IonQuant**. *A*, workflow to assess the quantification of IPIAA probes. *B*, heavy to light intensity ratios from 1:1 and 4:1 IPIAA-H: IPIAA-L mixtures aggregated from triplicate datasets (+FAIMS) using FragPipe coupled with IonQuant (FP) or ratios of integrated peak areas from ion chromatograms Skyline (SK), mean ratio values reported. *C*, FragPipe IonQuant ratio reproducibility with and without FAIMS using 1:10 IPIAA-H: IPIAA-L mixtures, mean ratio values reported. *Dashed lines* indicate ground-truth $\log_2$ ratio. Experiments were performed in triplicate for ± FAIMS comparisons and 4:1 comparisons and duplicate for 1:1 comparisons. Data available in supplemental Table S1. FAIMS, field asymmetric waveform ion mobility spectrometry; IPIAA, isopropyl iodoacetamide alkyne.

maximal ratio of 20 or minimal ratio of 1/20 (log2 values of ± 4.32).

To further benchmark and optimize the IonQuant quantification, we next established a pipeline for Skyline quantification of these model datasets. From FragPipe searches, interact.pep.xml files were imported into Skyline following the standard DDA analysis workflow for isotopically labeled dataset with the following modifications. As Skyline automatically places a heavy isotopic label on all modified cysteines, including carbamidomethylated residues and those modified by the IPIAA-H regent, quantification fails for peptides containing two or more modified cysteines (*e.g.*, one carbamidomethyl residue and one IPIAA-residue). Therefore, a custom plugin was generated to remove the heavy mass from all carbamidomethylated residues. Accurate quantification of FAIMS data was achieved using the Ion Mobility settings (See Supplementary Information). While Skyline initially outperformed IonQuant in terms of absolute numbers of peptides quantified (supplemental Fig. S5), we found that this difference in performance could be eliminated by adjusting the IonQuant parameters by setting minimum scan and minimum isotopes required for feature detection to 1 (supplemental Fig. S5). With these changes, we observed similar quantification with Skyline and IonQuant using our 1:1 and 4:1 datasets (Fig. 2*B*).

As FAIMS-based separation of peptides has only recently been implemented for chemoproteomics experiments (40) the impact of FAIMS on quantitation of detected ions in chemoproteomics experiments has not, to our knowledge, been explored. Therefore, our next step was to compare the relative intensities of peptide ratios of samples analyzed with and without FAIMS. After observing the increased ratio variability in the 1:10 datasets, we opted to compare quantitation for the 1:10 samples analyzed with and without FAIMS. This comparison revealed FAIMS-associated ratio compression consistent with that of reported Stable Isotope Labeling by Amino acids in Cell culture experiments, with more pronounced compression evident for the higher ratio 1:10 datasets in comparison to the 4:1 datasets (supplemental Fig. S4) (45). Interestingly, FAIMS nearly eliminates the large fraction of single-isotopic labeled quantified peptides in both our FragPipe and Skyline analysis (peptides with ratio L:H ratio values >3,000 in Skyline datasets) (Figs. 2*C* and S4). We also found that FAIMS data analyzed using FragPipe (mean ratio = −2.57) showed reduced ratio compression relative to Skyline quantitation with Ion Mobility settings (mean ratio= −1.79) (Fig. 2*C*), supporting the use of a FAIMS device coupled with IonQuant for quantitative chemoproteomic applications.

Single-Pot, Solid Phase-Enhanced Sample-Preparation for Identification of Relative Cysteine Oxidation and PTMProphet-Enabled Site-of-Labeling Localization

With heavy- and light-IPIAA probes in hand and quantitation workflow established, we next developed our chemoproteomic redox platform. Motivated by the improved coverage that we had achieved previously with SP3 solid phase sample cleanup, we tested whether the SP3 method could be extended to measure cysteine oxidation state with the goal of harnessing SP3-enabled repeated binding and elution on resin to conduct sequential capping, reduction, and capping steps with the heavy and light IPIAA probes.

We adapted the optimized workflow from our previous study to produce the SP3-Rox workflow, shown in Figure 3*A* (additional methodological details are shown in supplemental Fig. S6). Initial samples subjected to labeling in nondenaturing conditions indicated only partial or incomplete labeling of reduced cysteines in comparison to denaturing conditions with apparent ratio values nonrepresentative of a reduced thiol proteome (supplemental Fig. S7) (46, 47). To ensure optimal labeling, the samples were subjected to labeling with IPIAA-L in 2M urea first to cap all reduced cysteines; labeled proteins were then bound to SP3 resin and washed to remove excess IPIAA-L. Following on-SP3 resin thiol reduction and a second round of SP3 desalting to remove excess reductant, all formally oxidized cysteines were capped with IPIAA-H. The samples were then conjugated by CuAAC to biotin-azide, and excess reagents were removed by subsequent wash steps using SP3 beads. After sequence-specific digest (trypsin) and enrichment on neutravidin resin, labeled peptides were analyzed by LC-MS/MS. Notably, minimal lysis-induced oxidation was observed for both sonication and urea-based lysis (supplemental Fig. S8).

SP3-Rox analysis of Jurkat cell lysates in biological triplicate yielded 7,805 quantified cysteines in two or more replicates after filtering the data (Figs. 3, *A* and *B* and S9 and S10). SP3-Rox afforded robust (90–95%) enrichment of cysteine-containing peptides using this workflow, consistent with our previous study (40) (supplemental Fig. S11) and adequate peptide recovery from 400 μg input material (supplemental Fig. S12). Gratifyingly, and consistent with the aforementioned vetting of both Skyline and FragPipe quantitation, we observed a strong correlation between ratios reported for both methods, both with and without FAIMS (Figs. 3*B* and S10*A*). We also find that the median IonQuant H/L ratio is −3, (~10% oxidation) (supplemental Fig. S9), which is consistent with previously reported values for the median oxidation state of proteinaceous cysteines (46, 47). Analysis of annotated disulfides (UniProtKB) revealed a strong enrichment for higher heavy/light ratios anticipated for heavily oxidized thiols with a 3-fold increase in disulfide annotated cysteines for IonQuant $\log_2$(H/L) ratios > −3 (more than ~10% oxidized) in comparison to $\log_2$(H/L) ratios < −3. Notable disulfides identified include IGF2R Cys161, TF Cys137, CD1C Cys120, and HLA-A Cys188. Many disulfides with lower heavy/light ratios were found to be primarily in redox-active motifs (*e.g.*, thioredoxin, peroxiredoxin), which rationalizes the observed partial labeling by the IPIAA-L probe (Fig. 3*B*). We also observe modest FAIMS-induced ratio compression in comparison to samples run without FAIMS (supplemental Fig. S10*B*). To maintain

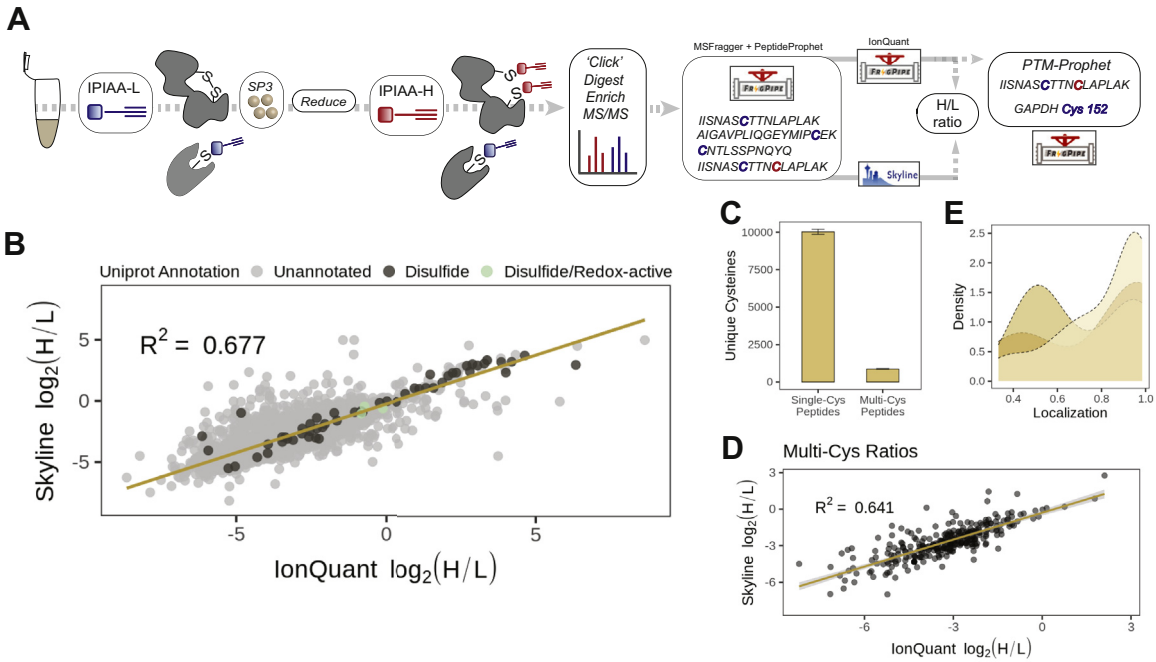

FIG. 3. **Application of SP3-Rox with FragPipe-IonQuant to identify oxidized cysteines**. *A*, workflow to assess the quantification of oxidation state ratios using SP3-Rox workflow. *B*, pairwise comparison of ratios quantified using FragPipe-IonQuant or Skyline aggregated from triplicate datasets; *dark color* indicates annotated disulfides, *green color* indicates annotated redox-active disulfides. *C*, comparison of single and multi-cysteine peptides aggregated from triplicate datasets. *D*, pairwise comparison of multi-cysteine peptide ratios using FragPipe-IonQuant or Skyline aggregated from triplicate datasets. *E*, localization scores on multi-cysteine peptides for three replicate experiments. Experiments were performed in triplicate. Data available in supplemental Table S2. IPIAA, isopropyl iodoacetamide alkyne; SP3, single-pot, solid-phase-enhanced sample-preparation.

consistency with previous studies, we provide both FragPipe reported ratios as well as a % oxidation metric in the proteomic datasets reported in supplemental Tables S2, S4, and S5.

Many redox-active cysteines are located in tryptic peptides that contain multiple cysteines. The accurate identification of the labeling site and quantification of the area ratio for these multi-cysteine containing peptides is confounded by several key factors. First, the default assumption of many software packages (*e.g.*, MaxQuant and Skyline) is that all cysteines within a given peptide are labeled by the same variable modification. Therefore, for methods that use multiple labels such as the SP3-Rox method, the identification and quantification of multi-cysteine peptides frequently fail using these software packages. To fix this issue, we implemented a customized plugin for Skyline analysis to compare multi-cysteine peptide ratios with those quantified by IonQuant in FragPipe. Second, as is the case with all posttranslational modifications, and described in detail for phosphoproteomics, identification of the labeling site for peptides containing multiple possible amino acid labeling sites can be confounded by the uncertainty caused by incomplete coverage of b and y ions (48). The lack of confidence metrics for posttranslational modification site assignments in most search engines makes differentiating these sites of labeling more difficult.

In contrast with other search algorithms, MSFragger has the flexibility to accommodate multiple unique modifications on cysteines. Six percentage of all unique peptides (over 450) quantified by the SP3-Rox method contain multiple cysteines (Fig. 3*C*). Of these, ~300 were found to contain light labeling together with carbamidomethyl modifications and only ~15 with both light and heavy labels. Comparison of the ratios generated for multi-cysteine containing peptides quantified by IonQuant and Skyline revealed a strong correlation, consistent with similar performance of both packages (Figs. 3*D* and S13). Analysis of individual Skyline MS1 peak areas for multi-cys peptides revealed high concordance with FragPipe identified ratios. Notably, partially labeled peptides containing one carbamidomethyl modification were observed to have substantially reduced intensities compared to fully labeled peptides, consistent with near complete IPIAA labeling afforded by the SP3-Rox method (supplemental Fig. S13). Validated against Skyline, we proceeded to use IonQuant for all subsequent analyses.

Using the PTMProphet tool (49) which is built into FragPipe and has recently been tailored to localize any assigned modifications, we assessed the probability score for localization and found that for most peptides, the localization probability is greater than 0.8 (Fig. 3*E*). Showcasing the accuracy of PTMProphet scoring, the known redox-active

cysteine Cys152 in GAPDH was identified with a light labeling and with carbamidomethyl labeling at Cys156 with localization scores ranging from 0.86 to 0.99 for each site (50). Similarly, for the Cys169, Cys171 multi-cys peptide from LYPLA1 thioesterase, Cys171 showed preferential light labeling with a localization score of 0.93. In contrast, a multi-cys peptide from the IKZF1 DNA-binding protein was identified with more ambiguous localization scores for the nonactive site, zinc-finger cysteines Cys147 and Cys150 positions (supplemental Table S2) (51).

SP3-Rox Identification of Cysteines Sensitive to Reversible Oxidation

Cysteine S-nitrosylation has been implicated in numerous biological processes, spanning apoptosis, proliferation, and angiogenesis and contributes to the pathology of multiple diseases (*e.g.*, Alzheimer's and Parkinson's disease) as well as host immune responses (7). Motivated by these wide ranging and significant biological impacts, we opted to apply our workflow to identify reversibly oxidized cysteines prone to S-nitrosation by GSNO (Fig. 4*A*). Immortalized T lymphocyte cell (Jurkat) proteome was treated with 1 mM GSNO or vehicle followed by SP3-Rox sample preparation to establish our method using samples with robust labeling. We identified 15,226 unique sites and 4,479 unique proteins using our workflow. 4,060 unique sites were identified in all four replicates per condition. The ratio difference between treated and control samples was then calculated for these 4,060 high confidence cysteines (Fig. 4*B*). Two thousand seventy two cysteines showed significant ratio changes (Difference >2, *p*-value < 0.5) sensitivity to GSNO labeling (Fig. 4*C*). Of these residues, a number with high ratio changes have been previously reported to be involved in the oxidative stress response including superoxide dismutase (SOD1 Cys147, ~6.3), parkin 7 (PARK7 Cys106, ~4.7), and thioredoxin (TXN Cys73, ~3.7) (Fig. 4*C*) (52–54). In particular, parkin 7 Cys106 oxidation is necessary for mitochondrial relocalization and protection against neuronal death (3, 55). The majority of Swiss-Prot reviewed and annotated S-nitrosocysteines identified in our dataset present significant and high ratio changes (Fig. 4*C*) (56).

Looking beyond proteins implicated in cellular response to oxidative stress, we next assessed whether other subsets of proteins were enriched for harboring redox sensitive cysteines. Gene ontology enrichment analysis (57, 58) of proteins exhibiting significant high ratio-change cysteines (residues highlighted in green, Fig. 4*B*) did not reveal enrichments in redox pathways, possibly due to the excess of GSNO (1 mM) used in our labeling study (supplemental Fig. S14). Immune-relevant proteins have been found to harbor numerous reactive and ligandable cysteines (59). Consistent with these findings, we uncovered a number of immune-relevant proteins containing GSNO-sensitive cysteines (supplemental Table S3).

Given that treatment with somewhat superphysiological concentrations of GSNO could easily afford nonspecific

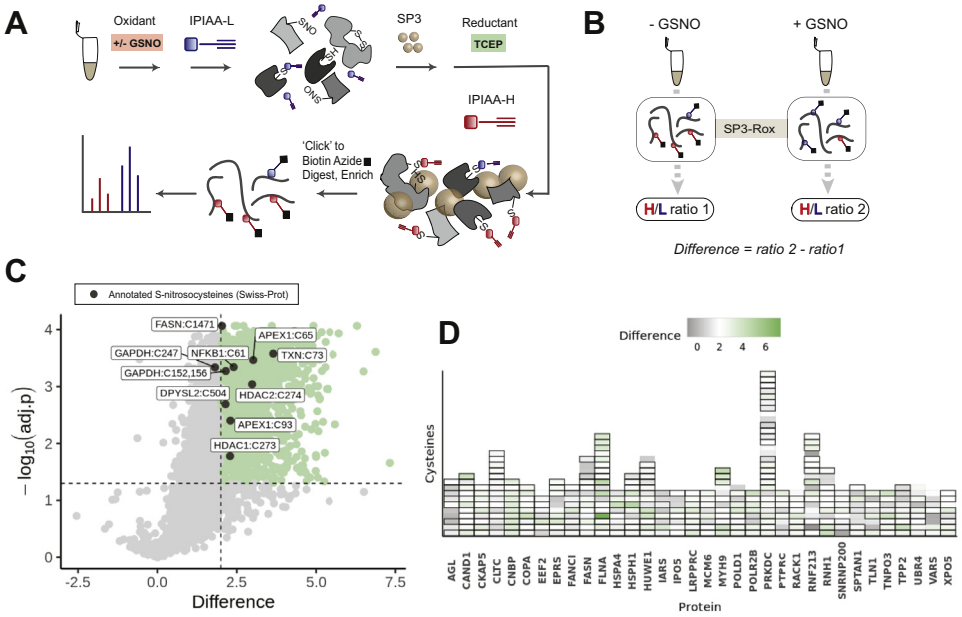

FIG. 4. **Application of SP3-Rox to identify redox-sensitive cysteines**. *A*, workflow to assess cysteines sensitive to nitrosation by GSNO. *B*, quantification of differential oxidation states. *C*, difference in mean $\log_2$ ratio upon GSNO treatment prior to labeling (Two-sample *t* test; *green* are significant Difference >2, *p*-value < 0.05 and *dark gray* are Swiss-Prot annotated S-nitrosocysteines; *p*-values adjusted using Benjamini–Hochberg procedure). *D*, heatmap showing $\log_2$ ratios of cysteines in multi-cys detected proteins, significant values bolded in gray. Experimental duplicates with two technical replicates (n = 4) were used for each treated and control condition. Data available in supplemental Table S4. GSNO, S-nitrosoglutathione; IPIAA, isopropyl iodoacetamide alkyne; SP3, single-pot, solid-phase-enhanced sample-preparation.

cysteine oxidation, we next asked whether SP3-Rox could stratify the relative GSNO sensitivity of individual cysteines. Across a panel of 50 proteins analyzed that all contain ≥ 6 quantified cysteines with significantly different ratio changes, we find that nearly all show preferential labeling of one or only a handful of cysteines across all residues detected (green, Fig. 4*D*). One notable exception is CNBP in which nearly all identified cysteines exhibit elevated ratios, consistent with nitrosylation. As CNBP contains multiple zinc finger motifs, we speculate that the observed GSNO promiscuous labeling is likely indicative of cysteine-modification-induced protein unfolding.

As redox-sensitive cysteines are frequently found in close proximity, both in sequence and 3D space, to additional cysteines, we hypothesized that the GSNO-sensitive cysteine subset would be enriched for peptides that contain multiple cysteines. We find that, of the sites we annotated as GSNO sensitive (Difference >2, p-value < 0.05), 6% belong to general multi-cys peptides (supplemental Fig. S15*A*) in comparison to 5% of sites we established as insensitive (Difference <2 or p-value > 0.05) (supplemental Fig. S15*B*). We then extended this analysis to the subset of peptides that contain a putative redox motif (either 'CXXC' or 'CXXXC'). In the GSNO-sensitive subset (green), nearly 40% of the multi-cys peptides contain a redox motif (supplemental Fig. S15*C*) compared to 28% in the insensitive subset (gray) (supplemental Fig. S15*D*). While we acknowledge that the relatively modest number of putative redox motif-containing peptides may preclude generalization of our findings, we believe that this observed enrichment highlights the importance of considering multi-cys motifs in quantification pipelines, particularly those aimed at profiling redox-sensitive cysteines.

SP3-Rox for Identification of Cell-State–Dependent Redox-Sensitive Cysteines

Reactive oxygen species have been extensively implicated in the activation of peripheral T cells. T cell activation requires ROS production; however, inappropriately high levels of ROS are proinflammatory and have been linked to DNA damage and cell death (60–64). Several oxidation-sensitive cysteines have been implicated in the regulation of appropriate T cell function (*e.g.*, residues in NRF2 and NFKB) (65, 66).

As T cells produce a burst of ROS during cellular activation, we postulated that a comparison of resting (unstimulated) *versus* activated (anti-CD3 and anti-CD28 stimulated) T cell redoxomes would reveal changes in the oxidation state of cysteines involved in cellular activation. To test this model, T cells isolated from healthy donor blood were subjected to the SP3-Rox workflow either before or after stimulation with immobilized anti-CD3 and anti-CD28 antibodies (Fig. 5*A*).

Using the IonQuant workflow illustrated in Figure 3*A* for stimulated and resting T cells, we quantified 13,411 total cysteines including 4,061 high confidence cysteines identified in all four replicates per condition. We also find 243 multi-cysteine containing peptides (~5%) with varying and quantifiable ratios (supplemental Fig. S16). We found 55 cysteines with significant changes in cysteine redox state during activation (Difference < -1.5 or >1.5) (Fig. 5, *A* and *B*). As expected, we primarily observe increases in mean ratios indicating an oxidizing environment relative to unstimulated T cells. As in the GSNO analysis, we detect many proteins with multiple quantified cysteines, including a subset that exhibit high difference values (Fig. 5*C*). Comparison to the prior chemoproteomic inventory of ligandable cysteines in T cells revealed 33 ligandable and redox-sensitive cysteines (Difference >1), with several high ratio-change cysteines including RRP1B Cys197 and RPS6KA5 Cys475, which provides additional clues for prioritization of residues for future small molecule probe development campaigns (Fig. 5*B*) (59).

Gratifyingly, we identified a number of cysteines in proteins with known involvement in adaptive immune response and T cell activation. Consistent with the important contributions of protein kinases, particularly serine-threonine kinases in T cell function (67), we detect cell-state–dependent cysteine-oxidation changes in multiple kinase cysteines demonstrating changes in oxidative state with differences in the 1.5 to 2.0 range. For example in PRKCQ, which is implicated in T cell receptor signaling, we identify Cys193 (Difference = 1.77) (68). In PRKDC, the DNA-dependent kinase involved in DNA damage repair and telomere stability, Cys1312 shows increased oxidation during T cell activation (Difference = 1.61) (Fig. 5*B*) (69). Interestingly, a prior study of cysteine dimethylfumarate sensitivity in native and activated T cells identified PRKDC (Cys4045) and PRKCQ (Cys14/17 and Cys322) (70). We also identify serine protein kinase ATM Cys2021 (Difference = 1.73) and bifunctional polynucleotide phosphatase/kinase PNKP Cys445 (Difference = 2.34) implicated in DNA damage response critical to T cells (71, 72).

Among the cysteines demonstrating very high ratio changes (>2.5) is GATOR complex protein MIOS Cys276 (Difference = 3.00), which indirectly positively regulates the mTORC pathway as well as GCN1 Cys1482 (Difference = 3.32), a positive regular of the EIF2AK4 kinase pathway, and E2F1 activator RRP1B Cys197 (Difference = 2.65) (73–75). We observe many nonkinase proteins also linked to T cell regulation and viral and tumor immune response such as SHMT2 Cys412, ITPKB Cys693, ZC3HAV1 Cys581, CTPS1 Cys216, and SERPINB9 Cys98 (76–80). Several proteins demonstrating high ratio changes do not have direct links to T cell activation and may play roles not yet elucidated. We also see a small number of cysteines with more reduced redox state upon stimulation including GADD45GIP1 Cys124, a negative regulator of cell-cycle progression (81), which is more reduced in activated T cells and upregulated during activation (82) as well as IRF2BP2 Cys521, an important transcriptional repressor typically down-regulated during T cell activation (83).

Altered protein abundance can complicate the interpretation of putative oxidative modification events identified by

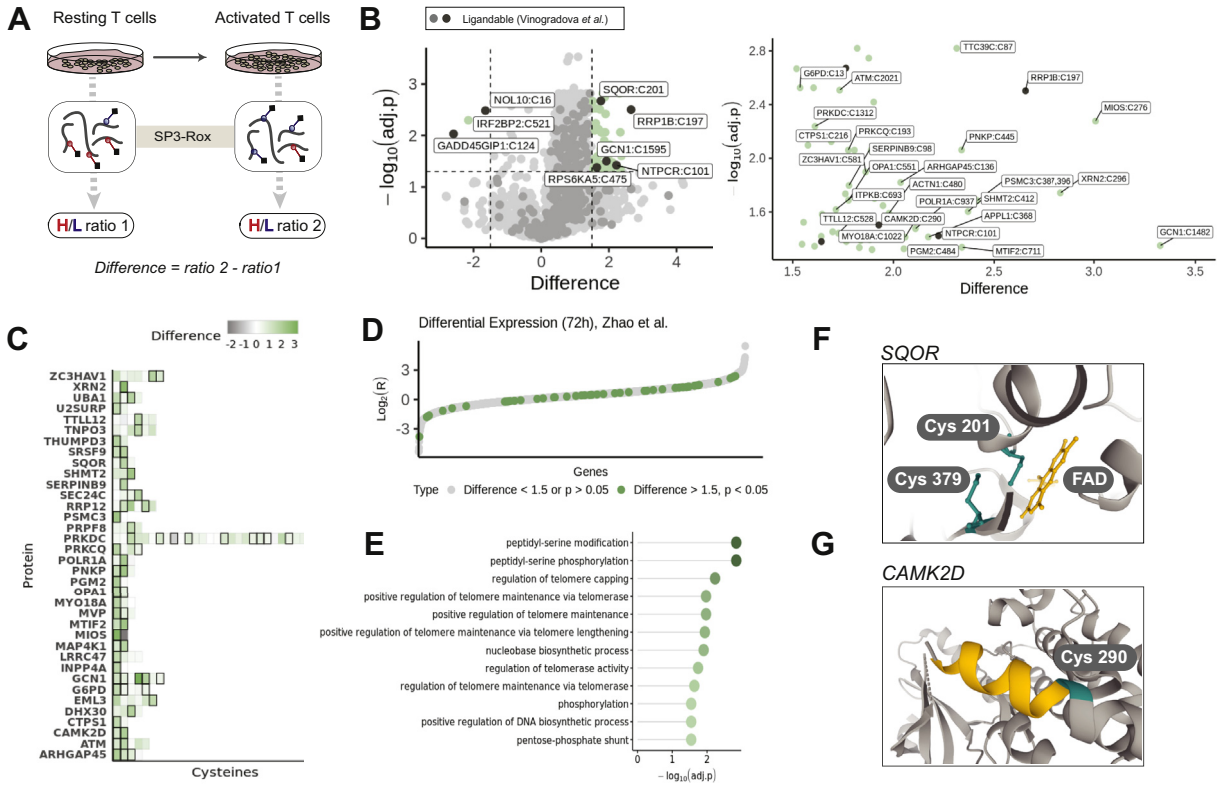

FIG. 5. **Application of SP3-Rox to identify redox changes during T cell maturation**. *A*, workflow to assess redox state in resting and activated T cells. *B*, difference in mean $\log_2$ ratio upon activation (Two-sample *t* test, *green* are significant Difference >1.5, *p*-value < 0.05; *darker gray* points are ligandable cysteines from Vinogradova *et al*.) (*left*), including immune-relevant cysteines indicated (*right*). *C*, heatmap showing $\log_2$ ratios of cysteines for proteins with multiple cysteines with at least one residue with significant Difference >1.5, significant values bolded in *gray*. *D*, comparison of differential expression for cysteines with Difference >1.5, *p*-value < 0.05 and all other cysteines using transcriptome datasets from Zhao *et al* (Mann-Whitney U test, *p*-value = 0.52). *E*, gene ontology-analysis of cysteines with Difference >1.5, *p*-value < 0.05 from panel B. *F*, crystal structure of SQOR indicating FAD-binding site and detected Cys201 and Cys379 (PDB 6OIB).*G*, crystal structure of CAMK2D indicating detected Cys290 and calmodulin-binding site (*yellow*) (PDB 5VLO). Experimental duplicates with two technical replicates (n = 4) were used for each treated and control condition. Data available in supplemental Table S5. SP3, single-pot, solid-phase-enhanced sample-preparation.

workflows requiring inter-sample ratio comparisons such as IsoTOP-ABPP and adaptations to the OxICAT method. A key advantage of the SP3-Rox method is its general insensitivity to abundance changes, even for proteins with only single cysteines identified. To further assess the ability of the SP3-Rox method to delineate oxidative modifications in the presence of expression changes, we analyzed unstimulated and activated T cell transcriptome profiling datasets from Zhao *et al*. to determine if significantly high ratio-change cysteine residues in Figure 5*B* reside in genes that show differential expression during activation. Comparing 0 h to 72 h differential expression datasets, we find that the subset of genes with high ratio-change (Difference >1.5) cysteines (green) show insignificant difference in the distribution of $\log_2$(R) values from all other genes (Fig. 5*D*).

Gene ontology-analysis of proteins that harbor cysteines with significant difference >1.5 revealed an enrichment for proteins involved in peptidyl-serine phosphorylation and telomere maintenance, consistent with well-established literature on loss of telomere length during T cell activation (84, 85) (Fig. 5*E*). Many identified cysteines reside in or near ATP-binding sites or enzyme active sites such as SQOR, which catalyzes the oxidation of hydrogen sulfide with active site Cys201 (Difference = 1.76), functioning as part of the catalytic disulfide bond (86) with Cys379. We also identify CAMK2D Cys290 (Difference = 2.06) near the calmodulin-binding site 291 to 301, which is intriguing given CAMK2D's roles in T cell proliferation (Fig. 5, *F* and *G*) (87).

DISCUSSION

Cysteine oxidative modifications are known to regulate most biological processes. Consequently, methods to determine the sites and fractional occupancy of thiol side chain modifications are widely applicable. Many such techniques are available including OxICAT, Cys-BOOST, and adaptations of IsoTOP-ABPP such as QTRP (10, 12, 87). Near ubiquitous-shared features of these methods are the requirement for multiple rounds of sample decontamination (typically

accomplished by precipitation or size exclusion) and for relatively large amounts of input material and for costly and complex isotopic reagents. Addressing these challenges, here, we combined new cost-effective isotopically labeled cysteine-reactive probes with SP3 sample cleanup to develop the SP3-Rox method, which is capable of quantifying cysteine oxidation state for small sample sizes, including for primary T cells derived from healthy donors.

To enable this method, we built upon our SP3 chemoproteomics sample cleanup workflow to incorporate two rounds of cysteine labeling, first capping all reduced cysteines and then all oxidized cysteines, with light and heavy isotopically differentiated iodoacetamide probes, respectively (40). While our method derives substantial inspiration from the pioneering OxICAT platform and workflows developed by Weerpana *et al*., the SP3-Rox method offers several clear advantages over these prior techniques. First, our reduced cost isotopically labeled IAA-reagents make subjecting samples to higher concentrations of reagents required for near complete capping of cysteines less cost prohibitive. Second, our use of SP3 sample cleanup streamlines standard redox preparation workflows by eliminating requirements for sample precipitation or other more laborious decontamination steps that frequently cause substantial material loss. As SP3 allows for repeated rounds of high yielding binding and elution to carboxyl-coated magnetic beads, samples can readily be capped, reduced, capped, and subjected to click chemistry, all in the same pot with minimal manipulation.

Critical to the success of the SP3-Rox method was our application of the FragPipe computational pipeline for highly sensitive peptide identification, as well as rigorous vetting of the FragPipe's built-in quantification module IonQuant by comparison with Skyline quantification. While proteomics tools such as FragPipe and Skyline have been widely adopted by the proteomics community, their use in chemoproteomics and redox proteomics has been limited to a handful of examples (40, 88, 89). Building upon our prior findings that MSFragger is compatible with search of chemoproteomics data generated using a FAIMS device for online fractionation, we first confirmed that search of samples labeled with the heavy and light IAA probes at a 1:1 stoichiometry afforded comparable PSMs for light- and heavy-labeled peptides. Next, we evaluated the performance of IonQuant and Skyline for quantification of samples labeled with different ratios to IAA probes (1:1, 4:1, 1:10), which revealed comparable performance for both quantification methods. Comparison of quantification for samples analyzed with and without FAIMS revealed improved quantification with FAIMS, albeit with modestly increased ratio compression. Of note, we find that FragPipe-processing affords less substantial FAIMS-induced compression when compared to Skyline. As chemoproteomics workflows have only recently incorporated online fractionation methods such as FAIMS, our work highlights the utility of FAIMS for simultaneously improving coverage and quantification of peptides detected in chemoproteomics studies. To enable widespread adoption of these free and versatile search and quantification tools by the chemoproteomics community, we provide a workflow file that automates implementation of our analysis pipeline (supporting file Sp3-Rox.workflow), and we include detailed step-by-step methods for our data analysis workflows.

We then combined our isotopically labeled IAA reagents, data analysis pipeline, and SP3 cleanup to generate the SP3-Rox method. Application of this method to Jurkat cell lysates identified 9,687 cysteines, including 219 known disulfides. In lysates subjected to 1 mM of the oxidant GSNO, we identified 2,072 oxidant-sensitive cysteines; follow-up studies should consider a dose-range of GSNO concentrations to mimic native cellular environments. One potential limitation of the SP3-Rox method is its reliance on a ratio-to-ratio comparison between oxidant and vehicle-treated samples, which may reduce the coverage of cysteines found in tough-to-detect peptides, including low abundance sequences and those that ionize poorly. This limitation is in part mitigated by the high coverage of the SP3-Rox method, which is achieved by our combination of Orbitrap Eclipse mass spectrometer (Thermo Scientific), FAIMS online fractionation, and enhanced coverage afforded by SP3 sample cleanup. One potential advantage of using relative ratio changes is the ability to control for any artificial oxidation introduced in sample preparation steps. The small and comparable amounts of methionine oxidation observed here for samples generated using two different lysis methods (sonication *versus* freeze/thaw lysis in urea) supports the generally minimal impact of artificial oxidation on our analyses (supplemental Fig. S8). In follow-up studies measuring general oxidation, steps should be taken to avoid artificial oxidation such as using mild and inactivating lysis conditions when possible.

Use of alternative methods, such as isoTOP-ABPP, which rely on competitive decrease in IAA labeling upon cysteine oxidation, provide a complementary alternative to the SP3-Rox method, with the possible advantage of increased coverage of tough-to-detect residues. However, such methods can be confounded by changes in protein abundance. In contrast, the SP3-Rox method and other related platforms should prove largely insensitive to expression-level changes, with the exception of complete activation or inactivation of a gene, and thus are well suited to applications where substantial proteome remodeling is expected. Furthermore, we expect that integration of the SP3-Rox method with probes tailored to capture specific oxidative modifications (*e.g.*, recently repurposed Wittig reagents (90)) likely will capture modification sites missed by *in vitro* labeling studies, which should prove particularly relevant for more labile or transient modifications.

Multiple redox active cysteines are often found in close proximity, both in peptide sequence and 3D space. Many search and quantification algorithms are not well equipped to

handle peptides containing multiple modifications. Addressing this issue, here, we show that FragPipe is capable of identifying multi-cysteine containing peptides with two or more different modifications and that IonQuant and Skyline both accurately quantify isotopic ratios of labeled peptides. We find that PTMProphet can be applied to score the confidence of labeling sites. Collectively, these findings provide a toolbox for the chemoproteomics community to enable rapid and accurate search and quantitation of chemoproteomics datasets, including for multi-cysteine containing peptides. While these multi-cysteine peptides represent a smaller fraction of all data, given their potential biological relevance, we anticipate that this localization data should prove useful for future studies aimed at functional annotation of the redox-sensitive cysteinome. Future efforts will include the incorporation of PTMProphet localizations in IonQuant quantification results.

Showcasing the utility of the SP3-Rox method, we apply our platform to identify cell-state dependent changes in cysteine oxidation. We find that during T cell activation, a number of cysteines show increased oxidation during cellular activation. As prior studies have demonstrated the contributions of low-level ROS to T cell activation and proliferation, we expect that a subset of the residues identified here are likely functional regulators of cellular activation. Although our workflow controls for protein abundance changes upon activation, we further used unmatched RNA-seq data to rule out confounding expression changes of genes harboring identified residues; future studies would benefit from matched transcriptomic data. The clinical relevance of cysteine-reactive molecules as immunomodulators points to future opportunities in the design and synthesis of tailored compounds aimed at targeting such functional residues (91). Future efforts to functionally validate the impact of these oxidative modifications should help to stratify functional and bystander oxidative modifications.

DATA AVAILABILITY

The MS data have been deposited to the ProteomeXchange Consortium (http://proteomecentral.proteomexchange.org/) *via* the PRIDE (92, 93) partner repository with the dataset identifiers PXD029500 and PXD031647. File and peptide details are listed in supplemental Table S6.

Supplemental data—This article contains supplemental data (28–30, 34, 38, 42, 43, 93, 94).

Acknowledgments—We thank all members of the Backus lab for helpful suggestions and the CFAR virology core 5P30 AI028697 for providing donor T cells as well as the UCLA Proteome Research Center for assistance with mass spectrometry-based proteomic data collection. We thank Nicholas Shulman for providing the custom Skyline plugin.

Funding and additional information—This study was supported by a Beckman Young Investigator Award (K. M. B.), V Scholar Award V2019-017 (K. M. B.), UCLA Jonsson Comprehensive Cancer Center Seed Grant (K. M. B.), TRDRP T31DT1800 (T. Y.), and the National Institutes of Health grant R01-GM-094231 (A. I. N.). The content is solely the responsibility of the authors and does not necessarily represent the official views of the National Institutes of Health.

Author contributions—H. S. D. and K. M. B. conceptualization; H. S. D., T. Y., and M. V. investigation; H. S. D. and T. Y. methodology; H. S. D. formal analysis; H. S. D. validation; H. S. D. and F. Y. data curation; H. S. D. visualization; H. S. D. and K. M. B writing–original draft; H. S. D., A. W. S., A. I. N., and K. M. B. writing–review and editing; A. W. S. resources; A. I. N. and K. M. B. supervision; A. I. N. and K. M. B. funding acquisition.

Conflicts of interest—The authors declare no competing interests.

Abbreviations—The abbreviations used are: CuAAC, copper-catalyzed azide–alkyne cycloaddition; FAIMS, field asymmetric waveform ion mobility spectrometry; GSNO, S-nitrosoglutathione; IA, iodoacetamide; IAA, iodoacetamide alkyne; IPIAA, isopropyl iodoacetamide alkyne; PSMs, peptide-spectrum matches; ROS, reactive oxygen species; RNS, reactive nitrogen species; SP3, single-pot, solid-phase-enhanced sample preparation; TCEP, tris(2-carboxyethyl) phosphine.

Received November 23, 2021, and in revised from, February 17, 2022 Published, MCPRO Papers in Press, February 25, 2022, https://doi.org/10.1016/j.mcpro.2022.100218

REFERENCES

1. Abo, M., and Weerapana, E. (2019) Chemical probes for redox signaling and oxidative stress. *Antioxid. Redox Signal.* **30**, 1369–1386
2. Backus, K. M. (2019) Applications of reactive cysteine profiling. In: Cravatt, B., Hsu, K. L., Weerapana, E., eds., **Vol. 420**. ,*Activity-Based Protein Profiling. Current Topics in Microbiology and Immunology*, Springer, Cham: 375–417
3. Fra, A., Yoboue, E. D., and Sitia, R. (2017) Cysteines as redox molecular switches and targets of disease. *Front. Mol. Neurosci.* **10**, 167
4. Cremers, C. M., and Jakob, U. (2013) Oxidant sensing by reversible disulfide bond formation. *J. Biol. Chem.* **288**, 26489–26496
5. D'Autréaux, B., and Toledano, M. B. (2007) ROS as signalling molecules: Mechanisms that generate specificity in ROS homeostasis. *Nat. Rev. Mol. Cell Biol.* **8**, 813–824
6. Sun, L., Wang, X., Saredy, J., Yuan, Z., Yang, X., and Wang, H. (2020) Innate-adaptive immunity interplay and redox regulation in immune response. *Redox Biol.* **37**, 101759
7. Paulsen, C. E., and Carroll, K. S. (2013) Cysteine-mediated redox signaling: Chemistry, biology, and tools for discovery. *Chem. Rev.* **113**, 4633–4679
8. Chouchani, E. T., James, A. M., Fearnley, I. M., Lilley, K. S., and Murphy, M. P. (2011) Proteomic approaches to the characterization of protein thiol modification. *Curr. Opin. Chem. Biol.* **15**, 120–128
9. Abo, M., Li, C., and Weerapana, E. (2018) Isotopically-labeled iodoacetamide-alkyne probes for quantitative cysteine-reactivity profiling. *Mol. Pharm.* **15**, 743–749

10. Fu, L., Li, Z., Liu, K., Tian, C., He, J., He, J., He, F., Xu, P., and Yang, J. (2020) A quantitative thiol reactivity profiling platform to analyze redox and electrophile reactive cysteine proteomes. *Nat. Protoc.* **15**, 2891–2919
11. García-Santamarina, S., Boronat, S., Domènech, A., Ayté, J., Molina, H., and Hidalgo, E. (2014) Monitoring *in vivo* reversible cysteine oxidation in proteins using ICAT and mass spectrometry. *Nat. Protoc.* **9**, 1131–1145
12. Leichert, L. I., Gehrke, F., Gudiseva, H. V., Blackwell, T., Ilbert, M., Walker, A. K., Strahler, J. R., Andrews, P. C., and Jakob, U. (2008) Quantifying changes in the thiol redox proteome upon oxidative stress *in vivo*. *Proc. Natl. Acad. Sci. U. S. A.* **105**, 8197–8202
13. Zhou, Y., Wynia-Smith, S. L., Couvertier, S. M., Kalous, K. S., Marletta, M. A., Smith, B. C., and Weerapana, E. (2016) Chemoproteomic strategy to quantitatively monitor transnitrosation uncovers functionally relevant S-nitrosation sites on Cathepsin D and HADH2. *Cell Chem. Biol.* **23**, 727–737
14. Guo, J., Gaffrey, M. J., Su, D., Liu, T., Camp, D. G., Smith, R. D., and Qian, W. J. (2013) Resin-assisted enrichment of thiols as a general strategy for proteomic profiling of cysteine-based reversible modifications. *Nat. Protoc.* **91**, 64–75
15. Xiao, H., Jedrychowski, M. P., Schweppe, D. K., Huttlin, E. L., Yu, Q., Heppner, D. E., Li, J., Long, J., Mills, E. L., Szpyt, J., He, Z., Du, G., Garrity, R., Reddy, A., Vaites, L. P., *et al*. (2020) A quantitative tissue-specific landscape of protein redox regulation during aging. *Cell* **180**, 968–983.e24
16. Jaffrey, S. R., and Snyder, S. H. (2001) The biotin switch method for the detection of S-nitrosylated proteins. *Sci. Signal.* **2001**. https://doi.org/10.1126/stke.2001.86.pl1
17. Lind, C., Gerdes, R., Hamnell, Y., Schuppe-Koistinen, I., Von Löwenhielm, H. B., Holmgren, A., and Cotgreave, I. A. (2002) Identification of S-glutathionylated cellular proteins during oxidative stress and constitutive metabolism by affinity purification and proteomic analysis. *Arch. Biochem. Biophys.* **406**, 229–240
18. Saurin, A. T., Neubert, H., Brennan, J. P., and Eaton, P. (2004) Widespread sulfenic acid formation in tissues in response to hydrogen peroxide. *Proc. Natl. Acad. Sci. U. S. A.* **101**, 17982–17987
19. Gygi, S. P., Rist, B., Gerber, S. A., Turecek, F., Gelb, M. H., and Aebersold, R. (1999) Quantitative analysis of complex protein mixtures using isotope-coded affinity tags. *Nat. Biotechnol.* **17**, 994–999
20. Ong, S. E., Blagoev, B., Kratchmarova, I., Kristensen, D. B., Steen, H., Pandey, A., and Mann, M. (2002) Stable isotope labeling by amino acids in cell culture, SILAC, as a simple and accurate approach to expression proteomics. *Mol. Cell Proteomics* **1**, 376–386
21. Vajrychova, M., Salovska, B., Pimkova, K., Fabrik, I., Tambor, V., Kondelova, A., Bartek, J., and Hodny, Z. (2019) Quantification of cellular protein and redox imbalance using SILAC-iodoTMT methodology. *Redox Biol.* **24**, 101227
22. Weerapana, E., Wang, C., Simon, G. M., Richter, F., Khare, S., Dillon, M. B. D., Bachovchin, D. A., Mowen, K., Baker, D., and Cravatt, B. F. (2010) Quantitative reactivity profiling predicts functional cysteines in proteomes. *Nature* **468**, 790–797
23. Shakir, S., Vinh, J., and Chiappetta, G. (2017) Quantitative analysis of the cysteine redoxome by iodoacetyl tandem mass tags. *Anal. Bioanal. Chem.* **409**, 3821–3830
24. Park, S. K., Venable, J. D., Xu, T., and Yates, J. R. (2008) A quantitative analysis software tool for mass spectrometry–based proteomics. *Nat. Methods* **54**, 319–322
25. Bae, J. W., Kim, S., Kim, V. N., and Kim, J. S. (2021) Photoactivatable ribonucleosides mark base-specific RNA-binding sites. *Nat. Commun.* **121**, 1–10
26. [preprint] Demichev, V., Yu, F., Teo, G. C., Szyrwiel, L., Rosenberger, G. A., Decker, J., Kaspar-Schoenefeld, S., Lilley, K. S., Mülleder, M., Nesvizhskii, A. I., and Ralser, M. (2021) High sensitivity dia-PASEF proteomics with DIA-NN and FragPipe. *bioRxiv*. https://doi.org/10.1101/2021.03.08.434385
27. Fisher, J., Mohanty, T., Karlsson, C. A. Q., Khademi, S. M. H., Malmström, E., Frigyesi, A., Nordenfelt, P., Malmstrom, J., and Linder, A. (2021) Proteome profiling of recombinant DNase therapy in reducing NETs and aiding recovery in COVID-19 patients. *Mol. Cell. Proteomics* **20**, 100113
28. Kong, A. T., Leprevost, F. V., Avtonomov, D. M., Mellacheruvu, D., and Nesvizhskii, A. I. (2017) MSFragger: Ultrafast and comprehensive peptide identification in mass spectrometry-based proteomics. *Nat. Methods* **14**, 513–520
29. Yu, F., Haynes, S. E., and Nesvizhskii, A. I. (2021) IonQuant enables accurate and sensitive label-free quantification with FDR-controlled match-between-runs. *Mol. Cell. Proteomics* **20**, 100077
30. Yu, F., Haynes, S. E., Teo, G. C., Avtonomov, D. M., Polasky, D. A., and Nesvizhskii, A. I. (2020) Fast quantitative analysis of timsTOF PASEF data with MSFragger and IonQuant. *Mol. Cell. Proteomics* **19**, 1575–1585
31. Yu, F., Teo, G. C., Kong, A. T., Haynes, S. E., Avtonomov, D. M., Geiszler, D. J., and Nesvizhskii, A. I. (2020) Identification of modified peptides using localization-aware open search. *Nat. Commun.* **111**, 1–9
32. Teo, G. C., Polasky, D. A., Yu, F., and Nesvizhskii, A. I. (2020) Fast deisotoping algorithm and its implementation in the MSFragger search engine. *J. Proteome Res.* **20**, 498–505
33. Van Gelder, K., Virta, L. K. A., Easlick, J., Prudhomme, N., McAlister, J. A., Geddes-McAlister, J., and Akhtar, T. A. (2021) A central role for polyprenol reductase in plant dolichol biosynthesis. *Plant Sci.* **303**, 110773
34. da Veiga Leprevost, F., Haynes, S. E., Avtonomov, D. M., Chang, H. Y., Shanmugam, A. K., Mellacheruvu, D., Kong, A. T., and Nesvizhskii, A. I. (2020) Philosopher: A versatile toolkit for shotgun proteomics data analysis. *Nat. Methods* **17**, 869–870
35. Day, N. J., Gaffrey, M. J., and Qian, W. J. (2021) Stoichiometric thiol redox proteomics for quantifying cellular responses to perturbations. *Antioxidants* **10**, 499
36. PT, C., KE, P., and RT, R. (1997) The CXXC motif: A rheostat in the active site. *Biochemistry* **36**, 4061–4066
37. Quan, S., Schneider, I., Pan, J., Von Hacht, A., and Bardwell, J. C. A. (2007) The CXXC motif is more than a redox rheostat. *J. Biol. Chem.* **282**, 28823–28833
38. Hughes, C. S., Moggridge, S., Müller, T., Sorensen, P. H., Morin, G. B., and Krijgsveld, J. (2019) Single-pot, solid-phase-enhanced sample preparation for proteomics experiments. *Nat. Protoc.* **14**, 68–85
39. Müller, T., Kalxdorf, M., Longuespée, R., Kazdal, D. N., Stenzinger, A., and Krijgsveld, J. (2020) Automated sample preparation with SP_3 for low-input clinical proteomics. *Mol. Syst. Biol.* **16**, e9111
40. Yan, T., Desai, H. S., Boatner, L. M., Yen, S. L., Cao, J., Palafox, M. F., Jami-Alahmadi, Y., and Backus, K. M. (2021) SP3-FAIMS chemoproteomics for high-coverage profiling of the human Cysteinome*. *Chembiochem* **22**, 1841–1851
41. Nesvizhskii, A. I. (2010) A survey of computational methods and error rate estimation procedures for peptide and protein identification in shotgun proteomics. *J. Proteomics* **73**, 2092–2123
42. MacLean, B., Tomazela, D. M., Shulman, N., Chambers, M., Finney, G. L., Frewen, B., Kern, R., Tabb, D. L., Liebler, D. C., and MacCoss, M. J. (2010) Skyline: An open source document editor for creating and analyzing targeted proteomics experiments. *Bioinformatics* **26**, 966–968
43. Backus, K. M., Correia, B. E., Lum, K. M., Forli, S., Horning, B. D., González-Páez, G. E., Chatterjee, S., Lanning, B. R., Teijaro, J. R., Olson, A. J., Wolan, D. W., and Cravatt, B. F. (2016) Proteome-wide covalent ligand discovery in native biological systems. *Nature* **534**, 570–574
44. Swearingen, K. E., and Moritz, R. L. (2012) High-field asymmetric waveform ion mobility spectrometry for mass spectrometry-based proteomics. *Expert Rev. Proteomics* **9**, 505–517
45. Pfammatter, S., Bonneil, E., McManus, F. P., and Thibault, P. (2019) Accurate quantitative proteomic analyses using metabolic labeling and high field asymmetric waveform ion mobility spectrometry (FAIMS). *J. Proteome Res.* **18**, 2129–2138
46. Hansen, R. E., Roth, D., and Winther, J. R. (2009) Quantifying the global cellular thiol–disulfide status. *Proc. Natl. Acad. Sci. U. S. A.* **106**, 422–427
47. Brandes, N., Reichmann, D., Tienson, H., Leichert, L. I., and Jakob, U. (2011) Using quantitative redox proteomics to dissect the yeast redoxome. *J. Biol. Chem.* **286**, 41893–41903
48. Kim, M. S., Zhong, J., and Pandey, A. (2016) Common errors in mass spectrometry-based analysis of post-translational modifications. *Proteomics* **16**, 700
49. Shteynberg, D. D., Deutsch, E. W., Campbell, D. S., Hoopmann, M. R., Kusebauch, U., Lee, D., Mendoza, L., Midha, M. K., Sun, Z., Whetton, A. D., and Moritz, R. L. (2019) PTMProphet: Fast and accurate mass modification localization for the trans-proteomic pipeline. *J. Proteome Res.* **18**, 4262–4272
50. Samson, A. L., Knaupp, A. S., Kass, I., Kleifeld, O., Marijanovic, E. M., Hughes, V. A., Lupton, C. J., Buckle, A. M., Bottomley, S. P., and

Medcalf, R. L. (2014) Oxidation of an exposed methionine instigates the aggregation of glyceraldehyde-3-phosphate dehydrogenase. *J. Biol. Chem.* **289**, 26922–26936
51. Hirano, T., Kishi, M., Sugimoto, H., Taguchi, R., Obinata, H., Ohshima, N., Tatei, K., and Izumi, T. (2009) Thioesterase activity and subcellular localization of acylprotein thioesterase 1/lysophospholipase 1. *Biochim. Biophys. Acta* **1791**, 797–805
52. Weichsel, Andrzej, Brailey, Jacqueline L., and Montfort, W. R. (2007) Buried S-nitrosocysteine revealed in crystal structures of human thioredoxin. *Biochemistry* **46**, 1219–1227
53. Arnesano, F., Banci, L., Bertini, I., Martinelli, M., Furukawa, Y., and O'Halloran, T. V. (2004) The unusually stable quaternary structure of human Cu, Zn-superoxide dismutase 1 is controlled by both metal occupancy and disulfide status. *J. Biol. Chem.* **279**, 47998–48003
54. Richarme, G., Mihoub, M., Dairou, J., Chi Bui, L., Leger, T., and Lamouri, A. (2015) Parkinsonism-associated protein DJ-1/park7 is a major protein deglycase that repairs methylglyoxal- and glyoxal-glycated cysteine, arginine, and lysine residues. *J. Biol. Chem.* **290**, 1885–1897
55. Canet-Avilés, R. M., Wilson, M. A., Miller, D. W., Ahmad, R., McLendon, C., Bandyopadhyay, S., Baptista, M. J., Ringe, D., Petsko, G. A., and Cookson, M. R. (2004) The Parkinson's disease protein DJ-1 is neuroprotective due to cysteine-sulfinic acid-driven mitochondrial localization. *Proc. Natl. Acad. Sci. U. S. A.* **101**, 9103–9108
56. Consortium, T. U., Bateman, A., Martin, M. J., Orchard, S., Magrane, M., Agivetova, R., Ahmad, S., Alpi, E., Bowler-Barnett, E. H., Britto, R., Bursteinas, B., Bye-A-Jee, H., Coetzee, R., Cukura, A., Da Silva, A., *et al*. (2021) UniProt: The universal protein knowledgebase in 2021. *Nucleic Acids Res.* **49**, D480–D489
57. Chen, E. Y., Tan, C. M., Kou, Y., Duan, Q., Wang, Z., Meirelles, G. V., Clark, N. R., and Ma'ayan, A. (2013) Enrichr: Interactive and collaborative HTML5 gene list enrichment analysis tool. *BMC Bioinformatics* **14**, 128
58. Kuleshov, M. V., Jones, M. R., Rouillard, A. D., Fernandez, N. F., Duan, Q., Wang, Z., Koplev, S., Jenkins, S. L., Jagodnik, K. M., Lachmann, A., McDermott, M. G., Monteiro, C. D., Gundersen, G. W., and Ma'ayan, A. (2016) Enrichr: A comprehensive gene set enrichment analysis web server 2016 update. *Nucleic Acids Res.* **44**, W90–W97
59. Vinogradova, E. V., Zhang, X., Remillard, D., Lazar, D. C., Suciu, R. M., Wang, Y., Bianco, G., Yamashita, Y., Crowley, V. M., Schafroth, M. A., Yokoyama, M., Konrad, D. B., Lum, K. M., Simon, G. M., Kemper, E. K., *et al*. (2020) An activity-guided map of electrophile-cysteine interactions in primary human T cells. *Cell* **182**, 1009–1026.e29
60. Angelini, G., Gardella, S., Ardy, M., Ciriolo, M. R., Filomeni, G., Trapani, G. D., Clarke, F., Sitia, R., and Rubartelli, A. (2002) Antigen-presenting dendritic cells provide the reducing extracellular microenvironment required for T lymphocyte activation. *Proc. Natl. Acad. Sci. U. S. A.* **99**, 1491–1496
61. Belikov, A. V., Schraven, B., and Simeoni, L. (2015) T cells and reactive oxygen species. *J. Biomed. Sci.* **22**, 1–11
62. Chen, X., Song, M., Zhang, B., and Zhang, Y. (2016) Reactive oxygen species regulate T cell immune response in the tumor microenvironment. *Oxid. Med. Cell Longev.* **2016**, 1580967
63. Sena, L. A., Li, S., Jairaman, A., Prakriya, M., Ezponda, T., Hildeman, D. A., Wang, C. R., Schumacker, P. T., Licht, J. D., Perlman, H., Bryce, P. J., and Chandel, N. S. (2013) Mitochondria are required for antigen-specific T cell activation through reactive oxygen species signaling. *Immunity* **38**, 225–236
64. Hildeman, D. A., Mitchell, T., Kappler, J., and Marrack, P. (2003) T cell apoptosis and reactive oxygen species. *J. Clin. Invest.* **111**, 575–581
65. Kesarwani, P., Murali, A. K., Al-Khami, A. A., and Mehrotra, S. (2013) Redox regulation of T-cell function: From molecular mechanisms to significance in human health and disease. *Antioxid. Redox Signal.* **18**, 1497–1534
66. Michalek, R. D., Nelson, K. J., Holbrook, B. C., Yi, J. S., Stridiron, D., Daniel, L. W., Fetrow, J. S., King, S. B., Poole, L. B., and Grayson, J. M. (2007) The requirement of reversible cysteine sulfenic acid formation for T cell activation and function. *J. Immunol.* **179**, 6456–6467
67. Navarro, M. N., and Cantrell, D. A. (2014) Serine-threonine kinases in TCR signaling. *Nat. Immunol.* **159**, 808–814
68. Isakov, N., and Altman, A. (2003) Protein kinase cθ in T cell activation. *Annu. Rev. Immunol.* **20**, 761–794
69. Mohiuddin, I. S., and Kang, M. H. (2019) DNA-PK as an emerging therapeutic target in cancer. *Front. Oncol.* **9**, 635
70. Blewett, M. M., Xie, J., Zaro, B. W., Backus, K. M., Altman, A., Teijaro, J. R., and Cravatt, B. F. (2016) Chemical proteomic map of dimethyl fumarate–sensitive cysteines in primary human T cells. *Sci. Signal.* **9**, rs10
71. Jilani, A., Ramotar, D., Slack, C., Ong, C., Yang, X. M., Scherer, S. W., and Lasko, D. D. (1999) Molecular cloning of the human gene, PNKP, encoding a polynucleotide kinase 3′-phosphatase and evidence for its role in repair of DNA strand breaks caused by oxidative damage. *J. Biol. Chem.* **274**, 24176–24186
72. Bhoumik, A., Takahashi, S., Breitweiser, W., Shiloh, Y., Jones, N., and Ronai, Z. (2005) ATM-dependent phosphorylation of ATF2 is required for the DNA damage response. *Mol. Cell* **18**, 577–587
73. Bar-Peled, L., Chantranupong, L., Cherniack, A. D., Chen, W. W., Ottina, K. A., Grabiner, B. C., Spear, E. D., Carter, S. L., Meyerson, M., and Sabatini, D. M. (2013) A tumor suppressor complex with GAP activity for the rag GTPases that signal amino acid sufficiency to mTORC1. *Science* **340**, 1100–1106
74. Cambiaghi, T. D., Pereira, C. M., Shanmugam, R., Bolech, M., Wek, R. C., Sattlegger, E., and Castilho, B. A. (2014) Evolutionarily conserved IMPACT impairs various stress responses that require GCN1 for activating the eIF2 kinase GCN2. *Biochem. Biophys. Res. Commun.* **443**, 592–597
75. Paik, J. C., Wang, B., Liu, K., Lue, J. K., and Lin, W. C. (2010) Regulation of E2F1-induced apoptosis by the nucleolar protein RRP1B. *J. Biol. Chem.* **285**, 6348–6363
76. Hayakawa, S., Shiratori, S., Yamato, H., Kameyama, T., Kitatsuji, C., Kashigi, F., Goto, S., Kameoka, S., Fujikura, D., Yamada, T., Mizutani, T., Kazumata, M., Sato, M., Tanaka, J., Asaka, M., *et al*. (2010) ZAPS is a potent stimulator of signaling mediated by the RNA helicase RIG-I during antiviral responses. *Nat. Immunol.* **121**, 37–44
77. Jiang, L., Wang, Y. J., Zhao, J., Uehara, M., Hou, Q., Kasinath, V., Ichimura, T., Banouni, N., Dai, L., Li, X., Greiner, D. L., Shultz, L. D., Zhang, X., Sun, Z. Y. J., Curtin, I., *et al*. (2020) Direct tumor killing and immunotherapy through anti-SerpinB9 therapy. *Cell* **183**, 1219–1233.e18
78. Ma, E. H., Bantug, G., Griss, T., Condotta, S., Johnson, R. M., Samborska, B., Mainolfi, N., Suri, V., Guak, H., Balmer, M. L., Verway, M. J., Raissi, T. C., Tsui, H., Boukhaled, G., Henriques da Costa, S., *et al*. (2017) Serine is an essential metabolite for effector T cell expansion. *Cell Metab.* **25**, 345–357
79. Martin, E., Palmic, N., Sanquer, S., Lenoir, C., Hauck, F., Mongellaz, C., Fabrega, S., Nitschké, P., Esposti, M. D., Schwartzentruber, J., Taylor, N., Majewski, J., Jabado, N., Wynn, R. F., Picard, C., *et al*. (2014) CTP synthase 1 deficiency in humans reveals its central role in lymphocyte proliferation. *Nature* **510**, 288–292
80. Pouillon, V., Hascakova-Bartova, R., Pajak, B., Adam, E., Bex, F., Dewaste, V., Van Lint, C., Leo, O., Erneaux, C., and Schurmans, S. (2003) Inositol 1, 3,4,5-tetrakisphosphate is essential for T lymphocyte development. *Nat. Immunol.* **4**, 1136–1143
81. Chung, H. K., Yi, Y. W., Jung, N. C., Kim, D., Suh, J. M., Kim, H., Park, K. C., Song, J. H., Kim, D. W., Hwang, E. S., Yoon, S. H., Bae, Y. S., Kim, J. M., Bae, I., and Shong, M. (2003) CR6-interacting factor 1 interacts with Gadd45 family proteins and modulates the cell cycle. *J. Biol. Chem.* **278**, 28079–28088
82. Zhao, S., Fung-Leung, W. P., Bittner, A., Ngo, K., and Liu, X. (2014) Comparison of RNA-seq and microarray in transcriptome profiling of activated T cells. *PLoS One* **9**, e78644
83. Sécca, C., Faget, D. V., Hanschke, S. C., Carneiro, M. S., Bonamino, M. H., de-Araujo-Souza, P. S., and Viola, J. P. B. (2016) IRF2BP2 transcriptional repressor restrains naive CD4 T cell activation and clonal expansion induced by TCR triggering. *J. Leukoc. Biol.* **100**, 1081–1091
84. Patrick, M. S., Cheng, N. L., Kim, J., An, J., Dong, F., Yang, Q., Zou, I., and Weng, N. P. (2019) Human T cell differentiation negatively regulates telomerase expression resulting in reduced activation-induced proliferation and survival. *Front. Immunol.* **10**, 1993
85. Röth, A., Yssel, H., Pène, J., Chavez, E. A., Schertzer, M., Lansdorp, P. M., Spits, H., and Luiten, R. M. (2003) Telomerase levels control the lifespan of human T lymphocytes. *Blood* **102**, 849–857
86. Jackson, M. R., Loll, P. J., and Jorns, M. S. (2019) X-ray structure of human sulfide:quinone oxidoreductase: Insights into the mechanism of mitochondrial hydrogen sulfide oxidation. *Structure* **27**, 794–805.e4
87. Mnatsakanyan, R., Markoutsa, S., Walbrunn, K., Roos, A., Verhelst, S. H. L., and Zahedi, R. P. (2019) Proteome-wide detection of S-nitrosylation

targets and motifs using bioorthogonal cleavable-linker-based enrichment and switch technique. *Nat. Commun.* **101**, 1–12

88. Yan, T., Palmer, A. B., Geiszler, D. J., Polasky, D. A., Armenta, E., Nesvizhskii, A. I., and Backus, K. M. (2021) *Enhancing Cysteine Chemoproteomic Coverage Through Systematic Assessment of Click Chemistry Product Fragmentation*
89. Zanon, P. R. A., Yu, F., Musacchio, P., Lewald, L., Zollo, M., Krauskopf, K., Mrdović, D., Raunft, P., Maher, T. E., Cigler, M., Chang, C., Lang, K., Toste, F. D., Nesvizhskii, A. I., and Hacker, S. M. (2021) Profiling the proteome-wide selectivity of diverse electrophiles. *ChemRxiv*. https://doi.org/10.26434/chemrxiv.14186561.v1
90. Shi, Y., Fu, L., Yang, J., and Carroll, K. S. (2021) Wittig reagents for chemoselective sulfenic acid ligation enables global site stoichiometry analysis and redox-controlled mitochondrial targeting. *Nat. Chem.* **2021**, 1–11
91. Backus, K. M., Cao, J., and Maddox, S. M. (2019) Opportunities and challenges for the development of covalent chemical immunomodulators. *Bioorg. Med. Chem.* **27**, 3421–3439
92. Deutsch, E. W., Csordas, A., Sun, Z., Jarnuczak, A., Perez-Riverol, Y., Ternent, T., Campbell, D. S., Bernal-Llinares, M., Okuda, S., Kawano, S., Moritz, R. L., Carver, J. J., Wang, M., Ishihama, Y., Bandeira, N., *et al*. (2017) The ProteomeXchange consortium in 2017: Supporting the cultural change in proteomics public data deposition. *Nucleic Acids Res.* **45**, D1100–D1106
93. Perez-Riverol, Y., Csordas, A., Bai, J., Bernal-Llinares, M., Hewapathirana, S., Kundu, D. J., Inuganti, A., Griss, J., Mayer, G., Eisenacher, M., Pérez, E., Uszkoreit, J., Pfeuffer, J., Sachsenberg, T., Yilmaz, Ş., *et al*. (2019) The PRIDE database and related tools and resources in 2019: Improving support for quantification data. *Nucleic Acids Res.* **47**, D442–D450
94. Chambers, M. C., Maclean, B., Burke, R., Amodei, D., Ruderman, D. L., Neumann, S., Gatto, L., Fischer, B., Pratt, B., Egertson, J., Hoff, K., Kessner, D., Tasman, N., Shulman, N., Frewen, B., *et al*. (2012) A cross-platform toolkit for mass spectrometry and proteomics. *Nat. Biotechnol.* **30**, 918–920